Intellectual disability and neurogenesis defects associated with increased turnover of an O-GlcNAcase variant

Florence Authier[1+], Benedetta Attianese[1+], Sergio Galan Bartual[1], Conor W. Mitchell[1,2], Andrew T. Ferenbach[1], Diane Doummar[3], Perrine Charles[4], Cyril Mignot[5], Boris Keren[4] and Daan M. F. van Aalten[1,2*]

[1]Department of Molecular Biology and Genetics, Aarhus University, Aarhus, DK

[2]Division of Molecular, Cell and Developmental Biology, School of Life Sciences, University of Dundee, Dundee, UK

[3]AP-HP Sorbonne Université, Service de Neuropédiatrie, Hôpital Armand-Trousseau, Paris, FR

[4]AP-HP Sorbonne Université, Département de Génétique, groupe hospitalier Pitié-Salpêtrière, Paris, FR

[5]AP-HP Sorbonne Université, Département de Génétique et Centre de référence Déficiences Intellectuelles de Causes Rares, Hôpital Armand-Trousseau et groupe hospitalier Pitié-Salpêtrière, Paris, FR

[+]These authors contributed equally to this work

*Correspondence to: daan@mbg.au.dk

Abstract

Intellectual Disability (ID) is characterised by substantial limitations in cognitive function and adaptive behaviour, affecting 1-3% of the population. Protein O-GlcNAcylation is a posttranslational modification of nucleocytoplasmic proteins regulated by two opposing enzymes: O-GlcNAc transferase (OGT) and O-GlcNAcase (OGA). Recently, missense mutations in *OGT* have been shown to segregate with ID, associated with compensatory reduction of OGA expression, although it is unclear whether this is mechanistically linked to the disease. Here, we report a patient with a K885N *de novo* missense mutation in the C-terminal pseudo histone acetyltransferase domain of OGA, associated with ID, infantile spasms and autism. While the K885N mutation does not affect protein stability or activity *in vitro*, this residue sits in the canonical GCN5 acetyltransferase family acceptor binding cleft. Strikingly, mouse embryonic stem cells edited to harbour the K885N mutation show increased OGA turnover and defects in neurogenesis. Taken together, these data suggest a link between missense mutations in OGA and ID.

Introduction

Protein O-GlcNAcylation is the dynamic posttranslational modification of serine and threonine residues with a single *N*-acetylglucosamine (GlcNAc) moiety. As opposed to phosphorylation, mediated by hundreds of kinases and phosphatases, O-GlcNAcylation is catalysed by only two enzymes: OGT, responsible for the addition of O-GlcNAc (1), and O-GlcNAcase (OGA), responsible for its removal (2). O-GlcNAcylation acts as a key regulator of important cellular processes and has been associated with pathological conditions including diabetes, neurodegeneration and cancer (3–6). O-GlcNAcylation has also been shown to be essential for embryogenesis and development. Deletion of either *OGT* or *OGA* causes lethality and developmental defects in mice (7–11). O-GlcNAcylation is particularly abundant in the brain (2,12,13), notably at synapses (14,15) and many O-GlcNAc proteins important for neurodevelopment and synaptic function have been identified by mass spectrometry, for instance SynGAP1, Bassoon, Piccolo and NMDA receptors (16,17). Taken together, this body of work suggests an important role for O-GlcNAcylation in development and function of the brain.

Recently, several *OGT* missense mutations have been identified and characterized in patients affected by a new neurodevelopmental disorder associated with intellectual disability, development delay and dysmorphic features, called OGT-linked Congenital Disorder of Glycosylation (OGT-CDG) (18–25). While this highlighted an important role of O-GlcNAcylation in neurodevelopment, the molecular mechanisms underlying the disease remain unknown. Interestingly, cell lines and mice edited to carry OGT-CDG variants have shown reduced OGA protein levels, suggesting the presence of a compensatory mechanism that might contribute to the syndrome (19,20,22,24,26). While abolition of OGA expression or activity results in perinatal lethality in mice, loss of OGA is well tolerated in *Drosophila melanogaster* (27). However, impaired OGA expression or activity in the fly leads to locomotion, habituation and synaptic morphology defects (27). Furthermore, *Oga*$^{+/-}$ mice display a deficit in spatial learning and memory associated synaptic plasticity defects (28). In addition, brain-specific deletion of *Oga* in mice leads to delayed development of the brain, altered cortical layering and microcephaly associated with enlargement of the brain ventricles. These animals also showed defects in neurogenesis with imbalance between cell proliferation and differentiation (10). Microcephaly and brain morphological defects have also been reported in OGT-CDG patients (18). In a GWAS study, SNPs in *MGEA5/OGA* have been associated with

intelligence and cognitive function (29). Taken together, these observations suggest that changes in OGA expression and/or activity could lead to neuronal defects through mechanisms that are currently unknown.

Human OGA (hOGA) is encoded by the meningioma-expressed antigen 5 (*MGEA5*) gene. There are two main splice variants of OGA: a long and a short isoform, named OGA-L and OGA-S, respectively. The OGA-L isoform is composed of an N-terminal glycoside hydrolase domain, a central stalk linker domain and a C-terminal pseudo-histone acetyltransferase (pHAT) domain, whereas the short isoform completely lacks the pHAT domain (30,31). The N-terminal catalytic domain is a member of the CAZy GH84 glycosyl hydrolase family, using a substrate-assisted catalytic mechanism to hydrolyse O-GlcNAc from proteins (32–34). The pHAT domain shares similarities with histone acetyl transferases of the GCN5 family and was originally thought to have acetyltransferase activity (35). Puzzlingly, the domain lacks the key amino acids required for acetyl-CoA binding, and is thus thought to be a “pseudo” histone acetyltransferase (36). Interestingly, the OGA-S isoform is only expressed until birth in rat brains whereas OGA-L is expressed throughout pre- and post-natal development with a peak of expression perinatally between postnatal day 0 and 5, suggesting a prominent postnatal role for the isoform containing the pHAT domain (37). While the structure of the OGA catalytic domain and associated mechanisms of substrate binding and catalysis have been determined (38,39), the structure and function of the pHAT domain remains largely unexplored.

Here we report a *de novo* missense mutation in the OGA pHAT domain, resulting in substitution of Lys885 for Asn, that segregates with infantile spasms and intellectual disability. The patient displays speech and learning disabilities associated with autistic features including impaired social interaction. While the K885N mutation does not affect protein folding or catalytic activity *in vitro*, the K885N mutation increases OGA turnover in genome edited mESCs cells, leading to reduced protein levels. Differentiation of mESCs to neurons reveals reduced expression of neuronal markers suggesting defects in early neurogenesis. Taken together, these data establish a link between an OGA missense mutation and neurodevelopment disorder.

Results and Discussion

A patient carrying an OGA missense mutation shows ID

A patient male in his late adolescence (defined as 13-18 years) was referred to our clinical genetics unit for etiological diagnosis of intellectual disability (ID). He is the child of healthy unrelated individuals with an uneventful family history. Maternal hypertension was noted during pregnancy. Birth occurred at 36 weeks of amenorrhea with normal parameters: weight 3440 g, length 49 cm, OFC 36 cm and Apgar scores of 10 at both 1 and 5 minutes. There were no neurodevelopmental concerns during the first year of life. The patient was in the 25th percentile age range for sitting alone, 10th percentile for walking independently (percentile range ages are defined according to World Health Organization (40)) and spoke disyllabic words from the age of 12 months. Infantile spasms, a rare type of epilepsy, started after 1 year old. EEG recordings showed hypsarrhythmia. Brain MRI was normal. The patient received vigabatrin and corticosteroid therapy with a quick effective outcome, as spasms disappeared and no other seizure type appeared in the following years. The parents noted psychomotor retardation and restlessness after the onset of epilepsy. However, language, motor and social skills progressed from the start of his middle childhood (defined as 6-12 years). The patient attended a class for children with special needs. He obtained a qualification and is currently engaged in a sheltered employment. Neuropsychological assessment during his middle childhood showed light/moderate ID (WISC-IV, FSIQ of 54, VCI 57, PRI 69, WMI 67, PSI 71), whilst an update in his early twenties showed a heterogeneous cognitive profile (WAIS, VCI 59, PRI 84, WMI 66, SPI 78). Finally, one seizure occurred at the beginning of his twenties, with no further EEG abnormalities.

Whole exome sequencing was performed on the patient to uncover the cause of ID and seizures. This revealed two potential candidate genes. A heterozygous missense mutation was identified in the *OGA* gene: Chr10(GRCh37):g.103546304T>A p.(Lys885Asn) (**Fig. 1A**). Sequence alignment revealed that K885 is highly conserved in vertebrates (**Fig. 1B)**. In addition, a homozygous variant of unknown significance in a splicing region of the *C2orf70* gene: NM_001105519.2:c.462-7C>G was also identified. Relatives were tested for both variants to assess inheritance. While the OGA K885N mutation is a *de novo* variant as it was absent in both parents and an unaffected sibling, the *C2orf70* variant was identified in both parents at heterozygous level suggesting parental inheritance. The *C2orf70* gene encodes a predicted uncharacterized FAM166C protein. Another missense variant for *C2orf70* has been previously reported in a

family with ID, yet also co-segregates with an additional variant in *ALDH18A1* (41), a known ID gene (42,43). A search in GnomAD indicated that the *OGA* gene is intolerant to missense variation (Z score = 3) and highly intolerant to loss of function variation (pLI score = 0.97) while the *C2orf70* gene appeared to be tolerant to variations (Z score = 0.02; pLI = 0), suggesting that the *C2orf70* variant is less likely to be pathogenic. To investigate the potential for a neurodevelopmental function of *C2orf70*, we measured C2orf70/Fam166C protein levels in mESCs cells and mouse brain tissues. While the protein was observed in brain tissues from adult animals (**Fig. S1A**), it was not detected in either mESCs (**Fig. S1B**) or brain tissues (**Fig. S1A**) from E15.5 embryos, suggesting that this protein has no functional role during pre-natal neurodevelopment. Taken together, these data show that we have identified a patient carrying a *de novo* missense mutation in *OGA* associated with infantile spasms and intellectual disability.

The K885N mutation sits in the conserved GCN5 family acceptor binding cleft

We wondered what effects the K885N mutation could have on the human pHAT structure. In the absence of an available human pHAT structure, we took advantage of the human OGA Alpha Fold model (entry O60502, per-residue model confidence score pLDDT ≥ 90) to analyse the putative pHAT structure (44). The pHAT fold belongs to the Gcn5-related acetyltransferase family and is nearly identical to the experimentally determined *Oceanicola granulosus* pHAT (*Og*pHAT) Gcn5-related structure (RMSD = 1.1 Å over 134 Cα atoms) (36). Superposition of the human pHAT model with the structure of a Gcn5 acetyltransferase from *Tetrahymena thermophila* (tGcn5) in complex with a P53 peptide (RMSD = 3.9 Å over 80 Cα atoms) (45) places the P53 peptide in a narrow cleft close to the human pHAT putative active site indicating that the pHAT might still be able to bind acceptor substrates using the equivalent cleft (**Fig. 1D)**. A further comparison between the tGcn5 active site and the pHAT putative active site reveals the presence of a glutamate (Glu879) in pHAT which occupies the same position as the *t*Gcn5 general catalytic base (Glu122) (46). Similarly, the *t*Gcn5 Tyr160, which is involved in the stabilisation of the water molecule that transports a proton from the acceptor reactive lysine to the general base is equivalent to the pHAT Tyr891 (46). However, as suggested previously (36), the pHAT domain contains residues that seem to preclude acetyl-CoA binding; first, the Asp853 (Arg135 in *t*Gcn5) which introduces a destabilising negative charge in the p-loop used by other Gcn5 family members to stabilise the acetyl-CoA pyrophosphate (47) and the Met735 (Glu76 in *t*Gcn5) which seems to clash with the acetyl-CoA molecule. Taking these

observations together it is unlikely that the pHAT binds acetyl-CoA and functions as an acetyltransferase despite having an intact putative catalytic centre.

We next analysed the K885N mutation in the context of the human pHAT model. The K885N mutation is placed at the C-terminus of the α7 helix at one of the cleft entrances. In *t*Gcn5, the same position (Asn163) has been suggested to participate in substrate stabilisation (45) but not catalysis (46). Taken together, these structural predictions suggest that the K885N mutation sits in the conserved GCN5 family acceptor binding cleft.

The K885N mutation does not affect OGA folding or catalytic activity

Pathogenic missense mutations often lead to misfolding and loss of function of the encoded protein (48). To evaluate whether the K885N mutation in OGA affects its overall folding, we recombinantly produced OGA, the catalytically defective OGA^{D175N}, and OGA^{K885N} in *E. coli*. We then measured their denaturing curves by differential scanning fluorimetry (DSF) (**Fig. S2A**). We did not observe significant changes in the OGA^{K885N} DSF denaturing profile or its melting temperature when compared with the OGA or the OGA^{D175N} proteins suggesting that the K885N mutation does not affect the overall folding of OGA or its thermal stability.

The OGA^{K885N} mutation lies in the pHAT domain of OGA, which despite not having any known catalytic activity, has previously been suggested to aid OGA catalytic activity (49). To investigate whether the K885N mutation affects OGA catalytic activity, we used the 4-methylumbelliferyl-β-*N*-acetylglucosamine (4MU-GlcNAc) substrate to assess the activity of the OGA and the OGA^{K885N} proteins using the OGA^{D175N} protein as a negative control. The experimental K_m and catalytic efficiency (k_{cat}/K_m) values for OGA and the OGA^{K885N} proteins were almost identical and very similar to previously published OGA catalytic data (K_m = 3.0 µM ± 0.3 µM for OGA and 2.9 µM ± 0.2 µM for OGA^{K885N}; k_{cat}/K_m = 1.3 x 10^{-6} $M^{-1}s^{-1}$ for OGA 2.0 x 10^{-6} $M^{-1}s^{-1}$ for OGA^{K885N}) suggesting that the K885N mutation does not affect catalysis (**Fig. S2B**). Taken together, these data indicate that the K885N mutation in the pHAT domain of OGA does not affect OGA folding or its catalytic activity.

OGA^{K885N} mESCs show reduced OGA levels due to increased protein turnover

We next generated mESCs carrying the OGA^{K885N} mutation using CRISPR/Cas9 genome editing. Three independent clones for each of the three genotypes $OGA^{+/+}$, $OGA^{K885N/+}$ and $OGA^{K885/K885N}$ were validated by sequencing (**Fig. 1C**) and used for further analysis. We first investigated the effect of the mutation on O-GlcNAc homeostasis. While $OGA^{+/+}$ and $OGA^{K885N/+}$ showed similar OGA (**Fig. 2A, C**) and OGT (**Fig. 2D, E)** protein levels, we observed a significant reduction in OGA protein levels in the $OGA^{K885N/K885N}$ clones (**Fig. 2A, C**). This reduction was not associated with changes in global O-GlcNAc levels (**Fig. 2A, B**) or OGT protein levels (**Fig. 2D, E**) in any of the three genotypes.

To investigate whether the reduction in OGA protein levels was due to changes in *Oga* transcription, we performed qPCR analysis. We observed similar *Oga* mRNA levels in the three genotypes (**Fig. 2F**) suggesting that the K885N mutation does not affect *Oga* transcript levels. Similarly, no changes in *Ogt* mRNA levels were observed in the three genotypes (**Fig. 2G**). Taken together, these data suggest that the K885N mutation leads to reduced OGA protein levels in mESCs.

To investigate whether the reduction in OGA protein levels is caused by increased OGA turnover in the mutant mESCs, we next performed a cycloheximide (CHX) pulse-chase experiment. $OGA^{+/+}$, $OGA^{K885N/+}$ and $OGA^{K885N/K885N}$ mESCs were treated with the protein synthesis inhibitor CHX and OGA protein levels were assessed over a 24 h period. $OGA^{+/+}$ cells showed stable protein levels of OGA until 16 h of CHX treatment. At 24 h, OGA protein levels were reduced by 41 % in $OGA^{+/+}$ cells. Unlike $OGA^{+/+}$ cells, both $OGA^{K885N/+}$ and $OGA^{K885N/K885N}$ cells showed an early decrease of OGA proteins levels at 4 h, and after 24h extended to 66 % and 79 % loss of OGA, respectively (**Fig. 2H, I**). Taken together, these data show that OGA^{K885N} mESCs show reduced OGA levels due to increased protein turnover.

OGA^{K885N} mESCs show neurogenesis defects

To investigate whether the K885N mutation impacts neurogenesis and thus underpins the neurological defects observed in the patient, mESCs were differentiated into neuronal precursor cells (NPCs) for 8 days and subsequently into neurons for another 8 days using an established two-step protocol (50). During the differentiation process, all three $OGA^{K885N/K885N}$ clones showed reduced viability after day 8 while no such evidence of growth and/or viability defects were observed when cells were grown in self-renewal conditions. Morphological observation at day 14 showed neuron-like structures with neurites and cell body extension in $OGA^{+/+}$ and $OGA^{K885N/+}$ clones (**Fig. 3A**) suggesting induction of neurogenesis in both genotypes. As $OGA^{K885N/K885N}$ clones showed poor viability with few cells showing neuron-like structures

(**Fig. 3A**), only $OGA^{+/+}$ (2 independent clones) and $OGA^{K885N/+}$ (3 independent clones) mESCs were used for further analysis. We first assessed the expression of pluripotency markers by qPCR analysis prior to differentiation and after 8 days of neurodifferentiation. Before differentiation, expression of *Oct4* and *Sox2* was similar in both $OGA^{+/+}$ and $OGA^{K885N/+}$ mESCs clones (**Fig. 3B, C**), whereas only the $OGA^{K885N/+}$ clones showed increased expression of *Nanog*, a transcription factor that is associated with stem cell self-renewal, although fluctuation in *Nanog* expression does not necessarily infer commitment to pluripotency (51) (**Fig. 3D**). Moreover, expression of all three pluripotency markers decreased after 8 days differentiation in both $OGA^{+/+}$ and $OGA^{K885N/+}$ (**Fig. 3B, C and D)** showing induction of differentiation in both genotypes.

We next evaluated neuronal differentiation efficiency by qPCR using markers of early neurogenesis at days 8 and 16. At day 8, we observed an increase in the expression of *Sox1* and *Pax6,* two major transcription factors involved in neurogenesis (52,53), in both $OGA^{+/+}$ and $OGA^{K885N/+}$ clones (**Fig. 3F and G**) suggesting that both genotypes differentiated towards a neuronal lineage. While a similar increase of *Pax6* expression levels was observed between $OGA^{+/+}$ and $OGA^{K885N/+}$ clones (**Fig. 3G**), the increase in *Sox1* expression was less marked in the $OGA^{K885N/+}$ clones compared to $OGA^{+/+}$ (**Fig. 3F**). At day 16, $OGA^{K885N/+}$ mESCs clones showed reduced mRNA expression levels of *Sox2*, *Pax6* and *NeuN*, a marker of post-mitotic neurons, compared to $OGA^{+/+}$ mESCs clones (**Fig. 3G, H, I**). No difference in mRNA expression of *Gfap* (**Fig. 3J**), an astrocyte marker, was observed between both genotypes at day 16. Taken together, these data suggest that while $OGA^{K885N/+}$ mESCs clones did commit to differentiation, the K885N mutation affects neurogenesis in mESCs.

The K885N mutation affects OGA protein levels during neurogenesis

We next investigated the effect of the K885N mutation on O-GlcNAc homeostasis during neurogenesis. At day 8, both $OGA^{+/+}$ and $OGA^{K885N/+}$ clones showed elevation of global O-GlcNAcylation, as well as elevated OGA and OGT protein levels compared to undifferentiated conditions. While no differences in global O-GlcNAcylation and OGA protein levels were observed between these two genotypes, $OGA^{K885N/+}$ clones showed reduced OGT protein levels compared to the $OGA^{+/+}$ clones (**Fig. 4A, B, E, F and J**). It is worth noting that in undifferentiated conditions, both *Oga* and *Ogt* mRNA levels were increased in the $OGA^{K885N/+}$ compared to $OGA^{+/+}$ without affecting their respective protein levels (**Fig. 4L and K**). Similarly, no difference in global O-GlcNAcylation levels was observed between both $OGA^{+/+}$ and $OGA^{K885N/+}$ clones after 16 days of neurodifferentiation (**Fig. 4C and G**). However, while OGT protein levels remained unchanged

between both genotypes despite an increase in mRNA levels (**Fig. 4D, I and L**), OGA$^{K885N/+}$ clones showed reduced OGA protein levels, but not mRNA levels, compared to OGA$^{+/+}$ clones after 16 days of neurodifferentiation (**Fig. 4C, H and K**). Taken together, these findings suggest that the K885N mutation affects OGA protein levels during neurogenesis without affecting O-GlcNAc homeostasis.

Concluding remarks

Advances in genome sequencing in recent years have accelerated the rate of identification of novel ID genes. Recently we, and others, have identified novel missense mutations in *OGT* that segregate with ID (18). While the mechanisms underlying OGT-CDG aetiology remain unclear, most of these OGT variants have been associated with reduced levels of OGA as an attempt to maintain O-GlcNAcylation homeostasis in human cell and mouse models (18,19,22,24,26). Although these findings suggest that reduction of OGA levels/activity may contribute to OGT-CDG aetiology, what neurologic processes are sensitive to loss of OGA remains unknown. Here we have reported a patient with infantile spasms, developmental delay and ID associated with a *de novo* missense mutation in the pHAT domain of OGA. While this variant co-segregates with another variant in the *C2orf70* gene of unknown function, this gene is not expressed during embryogenesis. Furthermore, we show that the OGA^{K885N} mutation alone is associated with neurogenesis defects in mESCs, suggesting that this mutation is the origin of the neurodevelopment symptoms found in the patient.

Our data show that the K885N mutation causes a reduction in OGA protein levels in mESCs in undifferentiated conditions and during neurogenesis. In undifferentiated conditions, the decrease of OGA levels only occurs in homozygous OGA$^{K885N/K885N}$ mESCs and was caused by increased turnover of the protein, suggesting the involvement of a posttranslational mechanism. An increase in OGA protein turnover was also observed in the heterozygous OGA$^{K885N/+}$ clones, combined with neurogenesis defects. Importantly, recent OGA structural analyses have revealed a tight dimer (39). It is possible that the formation of heterodimers explains how OGA$^{K885N/+}$ induces OGA turnover similarly to OGA$^{K885N/K885N}$ cells. Crucially, this is in agreement with the fact that the patient is also only heterozygous for the K885N mutation. While *Oga*$^{+/-}$ mice also showed neurodevelopment defects (28), heterozygous OGA$^{D285A/+}$ mice in which half of the O-GlcNAcase function is blocked, do not. However, OGA$^{D285A/D285A}$ mice show reduced brain size and enlargement of the brain ventricles, associated with increased OGA protein levels (11).

Previous studies have linked delayed neurogenesis and reduction of OGA levels in mESCs and mice (10,54). In accordance with these studies, reduced OGA levels in our $OGA^{K885N/+}$ mESCs resulted in reduced expression of transcription factors important for early neurogenesis, including *Sox1,* a marker of neuronal precursors. Similarly, mESCs treated with OGA targeting siRNA or Thiamet G, a potent OGA inhibitor, showed reduced generation of *Sox1* positive cells and decreased *Sox1* mRNA levels (54). Defects in neuronal precursor generation can lead to a decrease of neuronal cell formation in later stages of neurodifferentiation and subsequently to altered brain development and cognitive function. Decreases in neuronal precursor markers in the $OGA^{K885N/+}$ cells were associated with reduction in neuronal markers including *Sox2*, *Pax6* and *NeuN*. Interestingly *Sox2* and *Pax6*, two transcription factors crucial for neurogenesis, maintenance of proliferative state, and cell fate determination of neuronal stem cells towards neuronal lineage (55–58) have been shown to co-regulate neuronal gene expression during neurodevelopment (59). Together, these observations suggest that the OGA K885N mutation may affect neurogenesis through effects on the *Sox2*/*Pax6* axis. Further studies are needed to elucidate the mechanisms linking OGA and neurodevelopment defects.

OGT-CDG patients commonly exhibit moderate to severe ID, dysmorphic features and brain anomalies. The symptoms of the patient carrying the OGA K885N mutation are limited to mild cognitive impairment and episodic epilepsy events. Reduction in OGA levels is also observed in OGT-CDG variants in association with decrease O-GlcNAc levels due to defects in OGT activity/stability (18). Synergistic effects of both events may explain the severity of the OGT-CDG mutations. Previous studies have shown that a 50% reduction of OGA protein/activity levels in mice is not sufficient to alter global O-GlcNAc levels (9,11). Similarly, reduction of OGA levels in OGA^{K885N} mESCs were not associated with changes in global O-GlcNAc levels in mESCs before and after neurodifferentiation. This suggests that the defects observed in the mESCs may not be linked to reduction of O-GlcNAcase activity or O-GlcNAc homeostasis but rather point towards a role of the pHAT domain.

The function of the pHAT domain remains unclear. It shares a fold with the large GCN5 family of acetyltransferases, but our, and previous, structural analyses suggest that it is unlikely that the pHAT binds acetyl-CoA and functions as an acetyltransferase (36). However, the K885N mutation sits in the conserved GCN5 family acceptor binding cleft and most of the key residues required for catalysis are conserved. Intriguingly, a rationally designed point mutant in the putative active site has suggested a role for the pHAT domain in the generation of orexin neurons from mouse embryonic stem cells (60).

In conclusion, we have shown that a *de novo* missense mutation in the pHAT domain of OGA leads to neurodevelopmental defects, possibly through O-GlcNAc-independent mechanisms. Although the discovery of this mutation further supports an essential role for OGA in neurodevelopment and cognitive function, the mechanisms underlying the symptoms are still unknown. The identification of other patients with OGA variants as well as the generation of animal models recapitulating the neurodevelopmental symptoms are required to further uncover the underlying mechanisms linking OGA to intellectual disability.

Materials & Methods

The Comité de protection des personnes (CPP) ILE DE France VI (Genedefi - CPP 74-12) gave ethical approval for this work. The participant' parents provided written and informed consent.

Exome sequencing

Library preparation was performed using SeqCap EZ MedExome kit (RocheTechnologies) and sequencing was generated on a NextSeq 500 instrument (Illumina Inc.) according to the manufacturer's protocols. Both parents and the proband were analysed (trio exome sequencing). For data processing, raw reads were mapped to the human genome reference-build hg19 using the Burrows Wheeler Aligner (BWA MEM v0.717) alignment algorithm. The resulting binary alignment/map (BAM) files were further processed by Genome Analysis Tool Kit HaplotypeCaller (GATK HC v3.8). The VCF files were then annotated on Snpeff version 4.3T. Only coding non-synonymous and splicing variants were considered. Variant prioritization was conducted thanks to the transmission mode (*de novo*, autosomal recessive and X-linked), and the frequency of the variants in the GnomAD database.

Cell culture

AW2 mESCs derived from E14-TG2a.IV (129/Ola) ES cells were kindly donated from the MRC Centre for Regenerative Medicine, Institute for Stem Cell Research, University of Edinburgh (61) and cultured as previously described (19).

Generation of mutant mESC cell lines

Editing CRISPR reagents including pBABED and pX335 were prepared as previously described (62). Mouse embryonic stem cells were transfected using Lipofectamine 3000 (Invitrogen, according to manufacturer's instructions) with pBABED, pX335 and the repair templates coding for either the K885N mutation or the native lysine, to obtain $OGA^{+/+}$, $OGA^{K885N/+}$ and $OGA^{K885N/K885N}$ clones. After 24 h, transfected cells were selected using 1 µg/ml puromycin treatment for 2 days. Colonies from single cells that survived puromycin treatment were grown for 1-2 weeks, genotyped and sequenced to confirm the insertion of repair templates. Editing CRISPR reagents and primers sequences are listed in **Supplemental Table 1**.

Western blots

Proteins were extracted in RIPA lysis buffer supplemented with protease inhibitor cocktail (1:100 dilution; 535140-1SET; Merck) for 30 min on ice, centrifuged at 14,000 rpm for 20 min at 4 °C and protein concentration was determined with Pierce 660 nm protein assay (Thermo Scientific). *Cp*OGA treatment to assess the specificity of the anti-O-GlcNAc antibody was performed as previously described (11). Proteins were then separated on precast 4 to 12% NuPAGE Bis–Tris Acrylamide gels (Invitrogen) and transferred to a nitrocellulose membrane. Membranes were incubated with primary antibodies overnight at 4 °C or 3 h at room temperature. Anti-OGA (1:500 dilution; HPA036141; Sigma), anti-O-GlcNAc (RL2) (1:500 dilution; NB300-524, Novus Biologicals), anti-OGT (F-12) (1:1000 dilution; sc-74546; Santa Cruz), rabbit anti-C2orf70/FAM166C (1:1000 dilution; NBP2-82897; Novus Biologicals), rabbit anti-actin (1:2000 dilution; A2103; Sigma). IR680/800-labelled secondary antibodies (Licor) were used for detection. Blots were imaged using a DLx Odyssey infrared imaging system (Li-Cor), and signals were quantified using Image Studio Lite (Li-Cor) or Empiria Studio (Li-Cor). Results were normalized to the mean of each corresponding wild type ($OGA^{+/+}$) replicates set and represented as a fold change relative to $OGA^{+/+}$.

qPCR analysis

Total RNA was purified from cells using RNAeasy Kit (Qiagen), and then 0.5-1 µg of sample RNA was used for reverse transcription with the qScript cDNA Synthesis Kit (Quantabio). Quantitative PCR reactions were performed as previously described (11). Samples were assayed in biological replicates with technical triplicates using a BioRAD CFX Opus 384 Real-time PCR. Results were normalized to the mean of each corresponding $OGA^{+/+}$ replicate set and represented as a fold change relative to $OGA^{+/+}$. A list of primers used can be found in **Supplemental Table 2**.

Cycloheximide assay

mESCs cells were treated with cycloheximide (Cayman Chemical) at a final concentration of 20 µg/ml for 0, 4, 8, 16 and 24 h before lysis. DMSO was used as a control.

Neuronal differentiation of mESCs

mESCs were differentiated as described (50). Briefly, cells were plated into a non-adhesive bacterial dish in basal differentiation media I (DMEM/F12, 15% FBS, 1% NEAA and 0.1 mM 2ME) for 2 days to induce embryoid body formation. From day 2 to day 8, cells were treated with 1 µM retinoic acid (R2625; Sigma-

Aldrich) to obtain NPCs. From day 9 to day 16, cells were cultured in N2B27 media (50% DMEM/F12, 50% Neurobasal media,1% N2, 2% B27 and 0.1mM 2ME). Cells were harvested at day 8 and day 16 for further analysis.

Cloning

A PCR product encoding the residues 11-396 was produced from a pre-existing full-length codon-optimised clone of human OGA obtained from Genscript. This fragment was subcloned as a *Bam*HI-*Not*I fragment into the plasmid pHEXmangled, a plasmid based on the pGEX6P1 backbone with the GST and PreScission sites replaced by a 6His tag. The same full-length template was used to produce a PCR product encoding the residues 536 to the end of human OGA preceded by a start codon. This was cloned as a *Xho*I-*Bam*HI fragment into pLinker2, a plasmid based on pET28a but lacking any encoded tag or start codon. The D175N and K885N mutations were introduced into plasmids Hm h133 3 and L2P LEND respectively to generate plasmids Hm A17 1 and L2P 85HE 4 respectively. The mutagenesis was carried out based on the Quikchange site directed mutagenesis kit by Stratagene, but using KOD polymerase instead of Pfu. All inserts were confirmed by DNA sequencing.

Protein expression and purification

The OGA^{WT} , OGA^{K885N} and catalytic defective OGA^{D175N} proteins were obtained by co-transforming a plasmid containing the N-terminal region of OGA (11-396) with another plasmid containing the C-terminal region of the protein (535-end) as previously described by (39). Briefly, OGA^{K885} was obtained by combining the Hm hi13 3 plasmid with the L2P LEND plasmid, OGA^{K885N} was obtained by combining the Hm hi13 3 plasmid with the L2P 85HE plasmid and finally, the OGA^{D175N} protein was obtained by combining the Hm A171 plasmid with the L2P LEND plasmid. A list of proteins and associated tags and constructs boundaries can be found in **Supplemental Table 3**. All constructs, were transformed (or co-transformed, if needed) into *E. coli BL21(DE3)pLysS* for protein expression. Cell cultures were grown to an OD_{600} of 0.6 and induced with 300 mM IPTG at 16 ^{o}C overnight. The cultures were then harvested by centrifugation at 4 000 rpm for 20 min. Cells were resuspended in lysis buffer (25 mM Tris pH 7.5, 150 mM NaCl and 0.5 mM TCEP), supplemented with DNase, protease inhibitor cocktail (1 mM benzamidine, 0.2 mM PMSF and 5 µM leupeptin) and lysozyme and lysed using a French press device. Cell debris was removed by centrifugation and the supernatant was incubated with Ni-NTA beads for 2 h on a roller at 4 ºC. After an extensive wash

of the beads with the lysis buffer, the recombinant proteins were cleaved off the beads with PreScission protease at 4 ºC overnight. The cleaved proteins were then recovered from the beads, concentrated and loaded onto a 26/600 Superdex 200 column previously equilibrated with lysis buffer. Corresponding fractions were confirmed by SDS-PAGE, pooled, concentrated to 20 mg/ml, flash frozen in liquid nitrogen and stored at -80 ^{o}C until further use.

Differential scanning fluorometry

Differential Scanning Fluorometry denaturing profiles were recorded with a BioRAD CFX Opus 96 Real-time PCR configured for detecting FRET signals. Briefly; 10 µM protein was mixed with 10 µM SYPRO Orange (Invitrogen ref S6650, 5X final working concentration) in 50 mM HEPES, 150 mM NaCl pH 7.5. Final reaction volume was 20 µl. Experiments were performed in sextuplicate, and results were plotted and further analysed using GraphPad Prism.

OGA Catalytic Activity

Steady state kinetics of 4MU-GlcNAc (4-methylumbelliferyl-β-N-acetylglucosamine) were measured in buffer containing 25 mM HEPES (pH 7.5), with substrate concentrations ranging from 0 to 2 mM in three-fold dilutions. Reactions were performed with 2.5 nM enzyme in a 100 µl assay volume and at 37 °C. Product concentration (4-MU) was measured as fluorescence using a plate reader (Spectramax I3x) at an excitation wavelength of 365 nm and emission of 445 nm. Experiments were performed in triplicate, and Michaelis-Menten kinetics were analysed using GraphPad Prism.

Acknowledgements

This work was funded by a Wellcome Trust Investigator Award (110061), a Novo Nordisk Foundation Laureate award (NNF21OC0065969) and a Villum Fonden Investigator (00054496) to D.M.F.v.A. C.W.M. is funded by the BBSRC EASTBIO Doctoral Training Programme. We would like to thank Bartosz Kowalski for support with enzymatic assay.

Author contributions

F.A. and D.M.F.v.A conceived the study; F.A., B.A., S.G.B., C.W.M. performed experiments; A.T.F. performed molecular biology; C.M., D.D., and P.C. collected clinical data; B.K. performed genomic analysis; F.A., B. A., S.G.B. and D.M.F.v.A analysed data and F.A., S.G.B and D.M.F.v.A interpreted the data and wrote the manuscript with input from all authors.

Conflict of interest

The authors have no conflicts of interest to declare.

Figure legends

Figure 1: Generation of the O-GlcNAcase OGA^{K885N} knock-in mESCs cells.

(a) Schematic representation of OGA; blue: glycosyl hydrolase (GH) domain, yellow: stalk domain, and green: the pseudo-histone acetyltransferase (pHAT) domain. The K885 mutation site in the pHAT domain is in orange.

(b) Multiple sequence alignment using OGA sequences from *Homo sapience* (Human), *Mus musculus* (Mouse), *Bos taurus* (Cow), *Danio rerio* (Zebrafish) and *Xenopus laevis* (Frog). Lys885 is marked in green.

(c) Sequencing of genomic DNA from knock in wild type OGA$^{+/+}$, heterozygous OGA$^{K885N/+}$ and homozygous OGA$^{K885N/K885N}$ mESCs clones. The presence of single K885N point mutation (in red) in knock in clones. Silent mutations are in orange.

(d) Details of the superposition of the tGCN5 P53 peptide (green) and acetyl-CoA (yellow) on the AlphaFold human pHAT domain model (surface). The human pHAT, K885 and Y891 are represented as orange sticks.

Figure 2: The OGA^{K885N} mutation causes reduction of OGA protein levels due to increased turnover.

Data are represented as mean ± SD, n = 3 individual mESCs clones for all genotypes. Significance using a *t*-test is shown as * $p < 0.05$ and ** $p < 0.01$.

(a) Western blot of O-GlcNAc and OGA protein levels in OGA$^{+/+}$, OGA$^{K885N/+}$ and OGA$^{K885N/K885N}$ mESCs. Actin antibody was used as loading control.

(b) Quantification of O-GlcNAcylated proteins from the Western blot in panel a).

(c) Quantification of OGA protein levels from the Western blot in panel a).

(d) Western blot of OGT protein levels in OGA$^{+/+}$, OGA$^{K885N/+}$ and OGA$^{K885N/K885N}$ mESCs. Actin antibody was used as loading control.

(e) Quantification of OGT protein levels from the Western blot in panel d).

(f) Quantification of the Oga mRNA levels in OGA$^{+/+}$, OGA$^{K885N/+}$ and OGA$^{K885N/K885N}$ mESCs.

(g) Quantification of the Ogt mRNA levels in OGA$^{+/+}$, OGA$^{K885N/+}$ and OGA$^{K885N/K885N}$ mESCs.

(h) Western blot of OGA protein levels during CHX assay in OGA$^{+/+}$, OGA$^{K885N/+}$ and OGA$^{K885N/K885N}$ mESCs for the indicated time points. Actin antibody was used as loading control.

(i) Percentage of OGA protein levels from panel h).

Figure 3: OGA^{K885N} mutation affects neurogenesis.

Representative microscopy images **(a)** of OGA$^{+/+}$, OGA$^{K885N/+}$ and OGA$^{K885N/K885N}$ mESCs after 14 days of neurodifferentiation, at magnification 10x. Quantification of *Sox2* **(b)**, Oct4 **(c)**, Nanog **(d)**, Sox1 **(e)** and Pax6 **(f)** mRNA levels in OGA$^{+/+}$ and OGA$^{K885N/+}$ mESCs in undifferentiated conditions and after 8 days of neurodifferentiation. Quantification of *Sox2* **(g)**, Pax6 **(h)**, NeuN **(i)** and Gfap **(g)** mRNA levels in OGA$^{+/+}$ and OGA$^{K885N/+}$ mESCs after 16 days of neurodifferentiation. Data are represented as mean ± SEM, n = 2 or 3 individual mESCs clones for all genotypes.

Figure 4: The K885N mutation causes reduction of OGA protein levels during neurogenesis without affecting global O-GlcNAc homeostasis.

Data are represented as mean ± SEM, n = 2/3 individual mESCs clones for all genotypes.

(a) Western blot of O-GlcNAc and OGA protein levels in OGA$^{+/+}$ and OGA$^{K885N/+}$ in undifferentiated conditions and after 8 days of neurodifferentiation. GAPDH antibody was used as loading control.

(b) Western blot of OGT protein levels in OGA$^{+/+}$ and OGA$^{K885N/+}$ in undifferentiated conditions and after 8 days of neurodifferentiation. GAPDH antibody was used as loading control.

(c) Western blot of O-GlcNAc and OGA protein levels in OGA$^{+/+}$ and OGA$^{K885N/+}$ after 16 days of neurodifferentiation. GAPDH antibody was used as loading control.

(d) Western blot of OGT protein levels in OGA$^{+/+}$ and OGA$^{K885N/+}$ after 16 days of neurodifferentiation. GAPDH antibody was used as loading control.

(e) Quantification of O-GlcNAcylated proteins from the Western blot in panel a).

(f) Quantification of OGA proteins from the Western blot in panel a).

(g) Quantification of O-GlcNAcylated proteins from the Western blot in panel c).

(h) Quantification of OGA proteins from the Western blot in panel c).

(i) Quantification of OGT proteins from the Western blot in panel d).

(j) Quantification of OGT proteins from the Western blot in panel b).

(k) Quantification of *Oga* mRNA levels in OGA$^{+/+}$ and OGA$^{K885N/+}$ mESCs prior to differentiation and after 8 and 16 days of neurodifferentiation.

(I) Quantification of *Ogt* mRNA levels in $OGA^{+/+}$ and $OGA^{K885N/+}$ mESCs prior to differentiation and after 8 and 16 days of neurodifferentiation.

Supplementary figure legends

Supplementary Figure S1:

(a) Western blot of C2orf70/FAM166C protein levels in brain tissues from wild-type adult and E15.5 embryos mice. Actin antibody was used as loading control.

(b) Western blot of C2orf70/FAM166C protein levels in wild-type undifferentiated mESCs and brain from wild type adult mouse. Actin antibody was used as loading control.

Supplementary Figure S2: The pHAT K885N mutation does not affect OGA folding or catalytic activity

(a) Thermal denaturation profiles of OGA, OGA^{K885N} and OGA^{D175N} proteins. The T_m values from OGA (52.5 ± 0.4 °C), OGA^{K885N} (53.6 ± 0.5 °C) and OGA^{D175N} (51.4 ± 0.5 °C) were calculated as the fluorescence vs. the temperature function first derivative maximum peak. Each graph data point represents the averaged data from 6 replicates.

(b) Michaelis-Menten kinetics of the OGA and OGA^{K885N} constructs. The OGA kinetic values are, V_{max} = 2.9 ± 0.1 µM min^{-1} and K_M = 3.0 ± 0.3 µM while the OGA^{K885N} kinetic values are, V_{max} = 2.1 ± 0.1 µM min^{-1} and K_M = 2.9 ± 0.2 µM. Averaged data of 3 replicates is represented in the graph.

Supplementary Table 1: Sequences of reagents used for introducing the K885N mutation to *Oga* gene and genotyping of the mESCs.

Guide RNA Left for K885N	TTACTTCACAGAAAGCCCCC
Guide RNA Right for K885N	GGGGGCTTTCTGTGAAGTAA
DNA repair template for K885N	GAAATTTAGGAATAGATAAAGCTGTTACCTGTATTAAACACGGTT CAAATCTATATGATACACTTACTTACATTTAAAACATTTGTTTTATT TCTAGGCTCCCGGGGCGCCTTTTGCGAGGTAAGACCTGACGAC AATAGAATTCTCGAATTTTACAGCAAGTTAGGCTGTTTTGAAATT GCAAAAATGGAAGGATTTCCAAAGGATGTGGTTATACTTGGTCG AAGCCTGTGACACTTGTTGGTACTG
gDNA genotyping Reverse for K885N	GATCTGCTGCCGCTCCAGCTCCAG
gDNA genotyping Forward for	GGGTCTGATGCCCTCTTGTGGTGTG

K885N	
Sequencing for K885N	CAGTACCAACAAGTGTCACAGGC

Supplementary Table 2: Sequences of primers used for qPCR analysis.

List of Primers	**Sequence (5'->3')**
Actin b Forward	GATCAAGATCATTGCTCCTCCTG
Actin b Reverse	CAGCTCAGTAACAGTCCGCC
Sox2 Forward	GGAAAGGGTTCTTGCTGGGT
Sox2 Reverse	ACGAAAACGGTCTTGCCAGT
Oct4 Forward	GGTGGAACCAACTCCCGAGG
Oct4 Reverse	ACCTTTCCAAAGAGAACGCCC
Nanog Forward	TCTGATTCAGGGCTCAGCA
Nanog Reverse	ATGCGTTCACCAGATAGCCC
Sox1 Forward	GTACAGCCCCATCTCCAACT
Sox1 Reverse	CTCCGACTTGACCAGAGATCC
Pax6 Forward	CCTGGTTGGTATCCCGGGA
Pax6 Reverse	CCGCTTCAGCTGAAGTCGCA
NeuN Forward	GAAACCTCCTCGGACAGCA
NeuN Reverse	AGCTTTTCAACGGGTTCAGC
Gfap Forward	CGGAGACGCATCACCTCTG
Gfap Reverse	AGGGAGTGGAGGAGTCATTCG
Oga Forward	TGCAGTGGTTAGGGTGTCG
Oga Reverse	AGCAAACGCTGGAACTCTCC
Ogt Forward	CCCCCTGAGCCCTTCAAAAC
Ogt Reverse	TCGTTGGTTCTGTACTGTCGG

Supplementary Table 3: List of proteins with associated tags and construct boundaries.

Plasmid	Protein	Tag	Antibody resistance	Boundaries	Mutations
Hm hi13 3	WT OGA N-term	His	Ampicillin	11-396aa	-
L2P LEND	WT OGA C-term HAT	-	Kanamycin	535aa-End	-
Hm A171	OGA catalytic deficient mutant	His	Ampicillin	11-396aa	D175N
L2P 85HE4	OGA K885N mutant	-	Kanamycin	535aa-End	K885N

References

1. Kreppel LK, Hart GW. Regulation of a cytosolic and nuclear O-GlcNAc transferase. Role of the tetratricopeptide repeats. The Journal of biological chemistry. 1999/11/05 ed. 1999;274(45):32015–22.
2. Gao Y, Wells L, Comer FI, Parker GJ, Hart GW. Dynamic O-glycosylation of nuclear and cytosolic proteins: cloning and characterization of a neutral, cytosolic beta-N-acetylglucosaminidase from human brain. The Journal of biological chemistry. 2001/01/20 ed. 2001;276(13):9838–45.
3. Ma J, Hart GW. Protein O-GlcNAcylation in diabetes and diabetic complications. Expert Rev Proteomics. 2013 Aug;10(4):365–80.
4. Pratt MR, Vocadlo DJ. Understanding and exploiting the roles of O-GlcNAc in neurodegenerative diseases. Journal of Biological Chemistry [Internet]. 2023 Oct 30 [cited 2023 Nov 6];0(0). Available from: https://www.jbc.org/article/S0021-9258(23)02439-0/abstract
5. Wani WY, Ouyang X, Benavides GA, Redmann M, Cofield SS, Shacka JJ, et al. O-GlcNAc regulation of autophagy and α-synuclein homeostasis; implications for Parkinson's disease. Molecular Brain. 2017 Dec;10(1):32–32.
6. Slawson C, Hart GW. O-GlcNAc signalling: implications for cancer cell biology. Nature reviews Cancer. 2011/08/19 ed. 2011;11(9):678–84.
7. Shafi R, Iyer SP, Ellies LG, O'Donnell N, Marek KW, Chui D, et al. The O-GlcNAc transferase gene resides on the X chromosome and is essential for embryonic stem cell viability and mouse ontogeny. Proceedings of the National Academy of Sciences of the United States of America. 2000/05/10 ed. 2000;97(11):5735–9.
8. O'Donnell N, Zachara NE, Hart GW, Marth JD. Ogt-dependent X-chromosome-linked protein glycosylation is a requisite modification in somatic cell function and embryo viability. Molecular and cellular biology. 2004/01/30 ed. 2004;24(4):1680–90.
9. Keembiyehetty C, Love DC, Harwood KR, Gavrilova O, Comly ME, Hanover JA. Conditional Knock-out Reveals a Requirement for O-Linked N-Acetylglucosaminase (O-GlcNAcase) in Metabolic Homeostasis. The Journal of Biological Chemistry. 2015 Mar 3;290(11):7097.
10. Olivier-Van Stichelen S, Wang P, Comly M, Love DC, Hanover JA. Nutrient-driven O-linked N-acetylglucosamine (O-GlcNAc) cycling impacts neurodevelopmental timing and metabolism. Journal of Biological Chemistry. 2017;292(15):6076–85.
11. Muha V, Authier F, Szoke-Kovacs Z, Johnson S, Gallagher J, McNeilly A, et al. Loss of O-GlcNAcase catalytic activity leads to defects in mouse embryogenesis. The Journal of biological chemistry [Internet]. 2021 Jan 1 [cited 2022 Jul 21];296. Available from: https://pubmed.ncbi.nlm.nih.gov/33610549/
12. Okuyama R, Marshall S. UDP-N-acetylglucosaminyl transferase (OGT) in brain tissue: temperature sensitivity and subcellular distribution of cytosolic and nuclear enzyme. Journal of neurochemistry. 2003;86(5):1271–80.
13. Akimoto Y, Comer FI, Cole RN, Kudo A, Kawakami H, Hirano H, et al. Localization of the O-GlcNAc transferase and O-GlcNAc-modified proteins in rat cerebellar cortex. Brain Research. 2003 Mar 21;966(2):194–205.
14. Lagerlof O, Hart GW, Huganir RL. O-GlcNAc transferase regulates excitatory synapse maturity. Proceedings of the National Academy of Sciences of the United States of America. 2017/02/02 ed. 2017;114(7):1684–9.
15. Cole RN, Hart GW. Cytosolic O-glycosylation is abundant in nerve terminals. Journal of neurochemistry. 2001/12/12 ed. 2001;79(5):1080–9.
16. Vosseller K, Trinidad JC, Chalkley RJ, Specht CG, Thalhammer A, Lynn AJ, et al. O-Linked N-Acetylglucosamine Proteomics of Postsynaptic Density Preparations Using Lectin Weak Affinity Chromatography and Mass Spectrometry *. Molecular & Cellular Proteomics. 2006 May 1;5(5):923–34.
17. Khidekel N, Ficarro SB, Peters EC, Hsieh-Wilson LC. Exploring the O-GlcNAc proteome: direct identification of O-GlcNAc-modified proteins from the brain. Proceedings of the National Academy of Sciences of the United States of America. 2004/09/02 ed. 2004;101(36):13132–7.

18. Pravata VM, Omelková M, Stavridis MP, Desbiens CM, Stephen HM, Lefeber DJ, et al. An intellectual disability syndrome with single-nucleotide variants in O-GlcNAc transferase. European Journal of Human Genetics [Internet]. 2020 Feb; Available from: http://www.nature.com/articles/s41431-020-0589-9

19. Pravata VM, Muha V, Gundogdu M, Ferenbach AT, Kakade PS, Vandadi V, et al. Catalytic deficiency of O-GlcNAc transferase leads to X-linked intellectual disability. Proceedings of the National Academy of Sciences of the United States of America. 2019 Jul;116(30):14961–70.

20. Pravata VM, Gundogdu M, Bartual SG, Ferenbach AT, Stavridis M, Õunap K, et al. A missense mutation in the catalytic domain of O-GlcNAc transferase links perturbations in protein O-GlcNAcylation to X-linked intellectual disability. FEBS Letters. 2020 Feb 1;594(4):717–27.

21. Omelková M, Fenger CD, Murray M, Hammer TB, Pravata VM, Bartual SG, et al. An O-GlcNAc transferase pathogenic variant that affects pluripotent stem cell self-renewal [Internet]. bioRxiv; 2023 [cited 2023 Mar 17]. p. 2023.03.13.531514. Available from: https://www.biorxiv.org/content/10.1101/2023.03.13.531514v1

22. Vaidyanathan K, Niranjan T, Selvan N, Teo CF, May M, Patel S, et al. Identification and characterization of a missense mutation in the O-linked β-N-acetylglucosamine (O-GlcNAc) transferase gene that segregates with X-linked intellectual disability. The Journal of biological chemistry. 2017;292(21):8948–63.

23. Gundogdu M, Llabrés S, Gorelik A, Ferenbach AT, Zachariae U, van Aalten DMFF. The O-GlcNAc Transferase Intellectual Disability Mutation L254F Distorts the TPR Helix. Cell chemical biology. 2018 May;25(5):513-518.e4.

24. Willems AP, Gundogdu M, Kempers MJE, Giltay JC, Pfundt R, Elferink M, et al. Mutations in N-acetylglucosamine (O-GlcNAc) transferase in patients with X-linked intellectual disability. The Journal of Biological Chemistry. 2017/06/07 ed. 2017;292(30):12621–31.

25. Selvan N, George S, Serajee FJ, Shaw M, Hobson L, Kalscheuer V, et al. O-GlcNAc transferase missense mutations linked to X-linked intellectual disability deregulate genes involved in cell fate determination and signaling. The Journal of biological chemistry. 2018 Jul;293(27):10810–24.

26. Authier F, Ondruskova N, Ferenbach AT, McNeilly A, Aalten DMF van. Neurodevelopmental defects in a mouse model of O-GlcNAc transferase intellectual disability [Internet]. bioRxiv; 2023 [cited 2023 Oct 25]. p. 2023.08.23.554427. Available from: https://www.biorxiv.org/content/10.1101/2023.08.23.554427v1

27. Muha V, Fenckova M, Ferenbach AT, Catinozzi M, Eidhof I, Storkebaum E, et al. O-GlcNAcase contributes to cognitive function in Drosophila. Journal of Biological Chemistry. 2020 Feb;jbc.RA119.010312-jbc.RA119.010312.

28. Yang YR, Song S, Hwang H, Jung JH, Kim SJ, Yoon S, et al. Memory and synaptic plasticity are impaired by dysregulated hippocampal O-GlcNAcylation. Sci Rep. 2017 Apr 3;7:44921.

29. Savage JE, Jansen PR, Stringer S, Watanabe K, Bryois J, De Leeuw CA, et al. Genome-wide association meta-analysis in 269,867 individuals identifies new genetic and functional links to intelligence. Nature genetics. 2018 Jul 1;50(7):912–9.

30. Comtesse N, Maldener E, Meese E. Identification of a nuclear variant of MGEA5, a cytoplasmic hyaluronidase and a beta-N-acetylglucosaminidase. Biochem Biophys Res Commun. 2001 May 11;283(3):634–40.

31. Vocadlo DJ. O-GlcNAc processing enzymes: catalytic mechanisms, substrate specificity, and enzyme regulation. Curr Opin Chem Biol. 2012 Dec;16(5–6):488–97.

32. Rao FV, Dorfmueller HC, Villa F, Allwood M, Eggleston IM, van Aalten DM. Structural insights into the mechanism and inhibition of eukaryotic O-GlcNAc hydrolysis. The EMBO journal. 2006/03/17 ed. 2006;25(7):1569–78.

33. Macauley MS, Whitworth GE, Debowski AW, Chin D, Vocadlo DJ. O-GlcNAcase uses substrate-assisted catalysis: kinetic analysis and development of highly selective mechanism-inspired inhibitors. J Biol Chem. 2005 Jul 8;280(27):25313–22.

34. Drula E, Garron ML, Dogan S, Lombard V, Henrissat B, Terrapon N. The carbohydrate-active enzyme database: functions and literature. Nucleic Acids Res. 2022 Jan 7;50(D1):D571–7.

35. Toleman C, Paterson AJ, Whisenhunt TR, Kudlow JE. Characterization of the histone acetyltransferase (HAT) domain of a bifunctional protein with activable O-GlcNAcase and HAT activities. The Journal of biological chemistry. 2004/10/16 ed. 2004;279(51):53665–73.
36. Rao FV, Schuttelkopf AW, Dorfmueller HC, Ferenbach AT, Navratilova I, van Aalten DM. Structure of a bacterial putative acetyltransferase defines the fold of the human O-GlcNAcase C-terminal domain. Open biology. 2013/10/04 ed. 2013;3(10):130021–130021.
37. Liu Y, Li X, Yu Y, Shi J, Liang Z, Run X, et al. Developmental Regulation of Protein O-GlcNAcylation, O-GlcNAc Transferase, and O-GlcNAcase in Mammalian Brain. PLOS ONE. 2012 août;7(8):e43724.
38. Schimpl M, Schüttelkopf AW, Borodkin VS, Van Aalten DMF. Human OGA binds substrates in a conserved peptide recognition groove. The Biochemical journal. 2010;432(1):1–7.
39. Roth C, Chan S, Offen WA, Hemsworth GR, Willems LI, King DT, et al. Structural and functional insight into human O-GlcNAcase. Nat Chem Biol. 2017 Jun;13(6):610–2.
40. WHO Multicentre Growth Reference Study Group. WHO Motor Development Study: windows of achievement for six gross motor development milestones. Acta Paediatr Suppl. 2006 Apr;450:86–95.
41. Harripaul R, Vasli N, Mikhailov A, Rafiq MA, Mittal K, Windpassinger C, et al. Mapping autosomal recessive intellectual disability: combined microarray and exome sequencing identifies 26 novel candidate genes in 192 consanguineous families. Mol Psychiatry. 2018 Apr;23(4):973–84.
42. Koh K, Ishiura H, Beppu M, Shimazaki H, Ichinose Y, Mitsui J, et al. Novel mutations in the ALDH18A1 gene in complicated hereditary spastic paraplegia with cerebellar ataxia and cognitive impairment. J Hum Genet. 2018 Sep;63(9):1009–13.
43. Magini P, Marco-Marin C, Escamilla-Honrubia JM, Martinelli D, Dionisi-Vici C, Faravelli F, et al. P5CS expression study in a new family with ALDH18A1-associated hereditary spastic paraplegia SPG9. Ann Clin Transl Neurol. 2019 Jul 19;6(8):1533–40.
44. Jumper J, Evans R, Pritzel A, Green T, Figurnov M, Ronneberger O, et al. Highly accurate protein structure prediction with AlphaFold. Nature. 2021 Aug;596(7873):583–9.
45. Poux AN, Marmorstein R. Molecular Basis for Gcn5/PCAF Histone Acetyltransferase Selectivity for Histone and Nonhistone Substrates,. Biochemistry. 2003 Dec 1;42(49):14366–74.
46. Rojas JR, Trievel RC, Zhou J, Mo Y, Li X, Berger SL, et al. Structure of Tetrahymena GCN5 bound to coenzyme A and a histone H3 peptide. Nature. 1999 Sep 2;401(6748):93–8.
47. Dyda F, Klein DC, Hickman AB. GCN5-related N-acetyltransferases: a structural overview. Annu Rev Biophys Biomol Struct. 2000;29:81–103.
48. Puglisi R. Protein Mutations and Stability, a Link with Disease: The Case Study of Frataxin. Biomedicines. 2022 Feb 11;10(2):425.
49. Li J, Huang C luan, Zhang L wen, Lin L, Li Z hua, Zhang F wu, et al. Isoforms of human O-GlcNAcase show distinct catalytic efficiencies. Biochemistry Moscow. 2010 Jul;75(7):938–43.
50. Mao X, Zhao S. Neuronal Differentiation from Mouse Embryonic Stem Cells In vitro. J Vis Exp. 2020 Jun 2;(160).
51. Xenopoulos P, Kang M, Puliafito A, Di Talia S, Hadjantonakis AK. Heterogeneities in Nanog Expression Drive Stable Commitment to Pluripotency in the Mouse Blastocyst. Cell Reports. 2015 Mar 10;10(9):1508–20.
52. Pevny LH, Sockanathan S, Placzek M, Lovell-Badge R. A role for SOX1 in neural determination. Development. 1998 May 15;125(10):1967–78.
53. Sansom SN, Griffiths DS, Faedo A, Kleinjan DJ, Ruan Y, Smith J, et al. The level of the transcription factor Pax6 is essential for controlling the balance between neural stem cell self-renewal and neurogenesis. PLoS Genet. 2009 Jun;5(6):e1000511.
54. Speakman CM, Domke TC, Wongpaiboonwattana W, Sanders K, Mudaliar M, van Aalten DM, et al. Elevated O-GlcNAc levels activate epigenetically repressed genes and delay mouse ES cell differentiation without affecting naive to primed cell transition. Stem cells [Internet]. 2014/06/06 ed. 2014; Available from: http://www.ncbi.nlm.nih.gov/pubmed/24898611
55. Kikkawa T, Casingal CR, Chun SH, Shinohara H, Hiraoka K, Osumi N. The role of Pax6 in brain development and its impact on pathogenesis of autism spectrum disorder. Brain Res. 2019 Feb 15;1705:95–103.

56. Tomas-Roca L, Qiu Z, Fransén E, Gokhale R, Bulovaite E, Price DJ, et al. Developmental disruption and restoration of brain synaptome architecture in the murine Pax6 neurodevelopmental disease model. Nat Commun. 2022 Nov 11;13(1):6836.
57. Mercurio S, Serra L, Pagin M, Nicolis SK. Deconstructing Sox2 Function in Brain Development and Disease. Cells. 2022 May 10;11(10):1604.
58. Amador-Arjona A, Cimadamore F, Huang CT, Wright R, Lewis S, Gage FH, et al. SOX2 primes the epigenetic landscape in neural precursors enabling proper gene activation during hippocampal neurogenesis. Proceedings of the National Academy of Sciences. 2015 Apr 14;112(15):E1936–45.
59. Thakurela S, Tiwari N, Schick S, Garding A, Ivanek R, Berninger B, et al. Mapping gene regulatory circuitry of Pax6 during neurogenesis. Cell Discov. 2016 Feb 9;2(1):1–22.
60. Hayakawa K, Hirosawa M, Tabei Y, Arai D, Tanaka S, Murakami N, et al. Epigenetic Switching by the Metabolism-sensing Factors in the Generation of Orexin Neurons from Mouse Embryonic Stem Cells. The Journal of Biological Chemistry. 2013 Jun 6;288(24):17099.
61. Zhou X, Smith AJH, Waterhouse A, Blin G, Malaguti M, Lin CY, et al. Hes1 desynchronizes differentiation of pluripotent cells by modulating STAT3 activity. Stem Cells. 2013 Aug;31(8):1511–22.
62. Gorelik A, Bartual SG, Borodkin VS, Varghese J, Ferenbach AT, van Aalten DMF. Genetic recoding to dissect the roles of site-specific protein O-GlcNAcylation. Nature structural & molecular biology. 2019;26(11):1071–7.

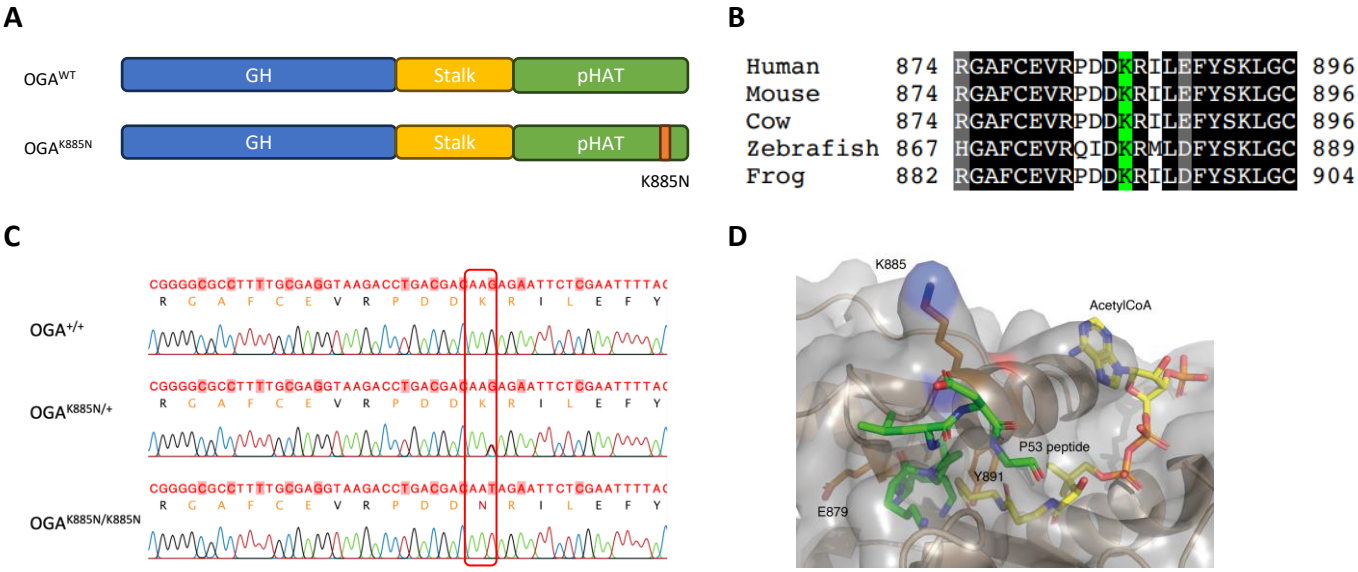

Fig. 1

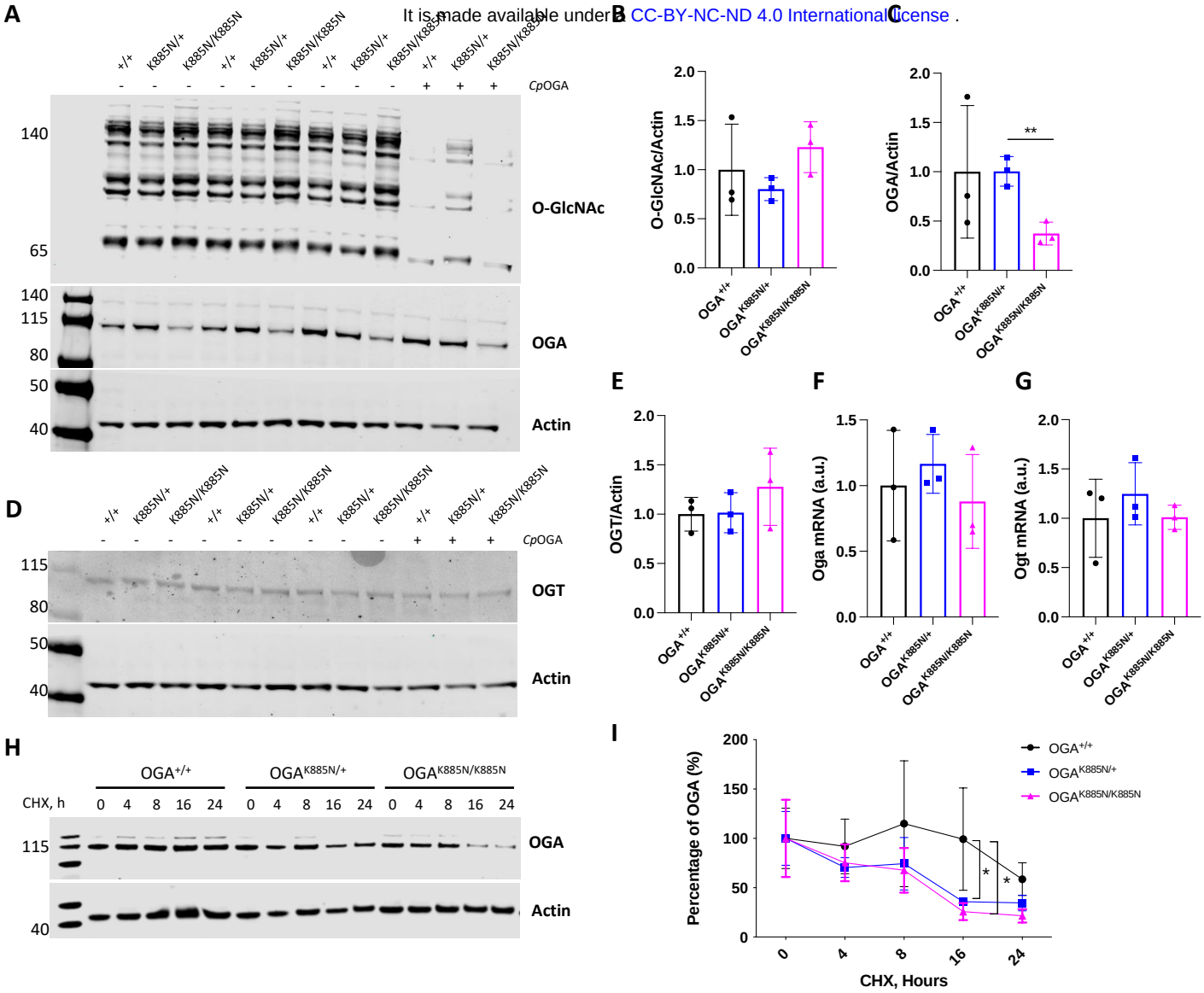

Fig. 2

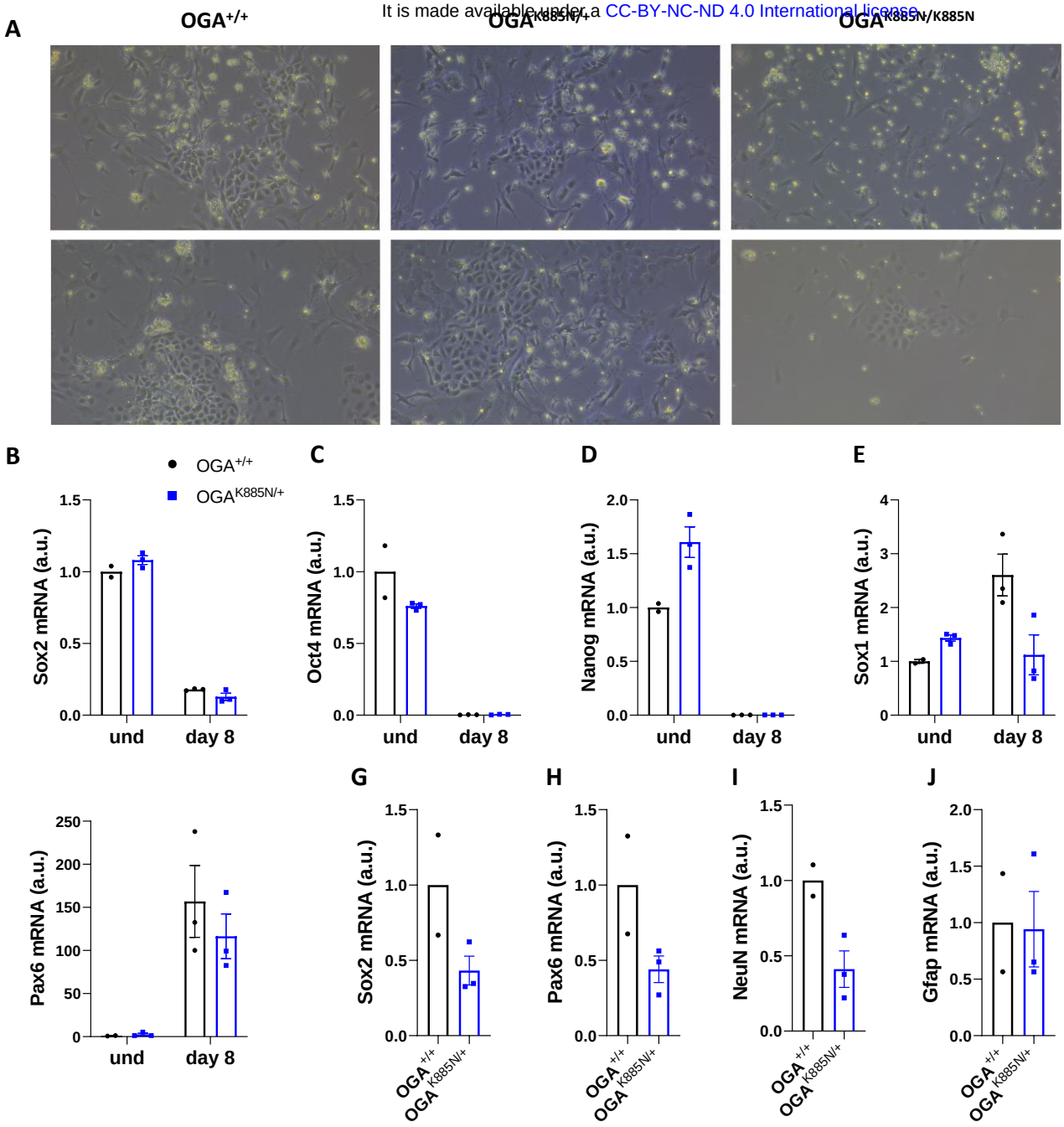

Fig. 3

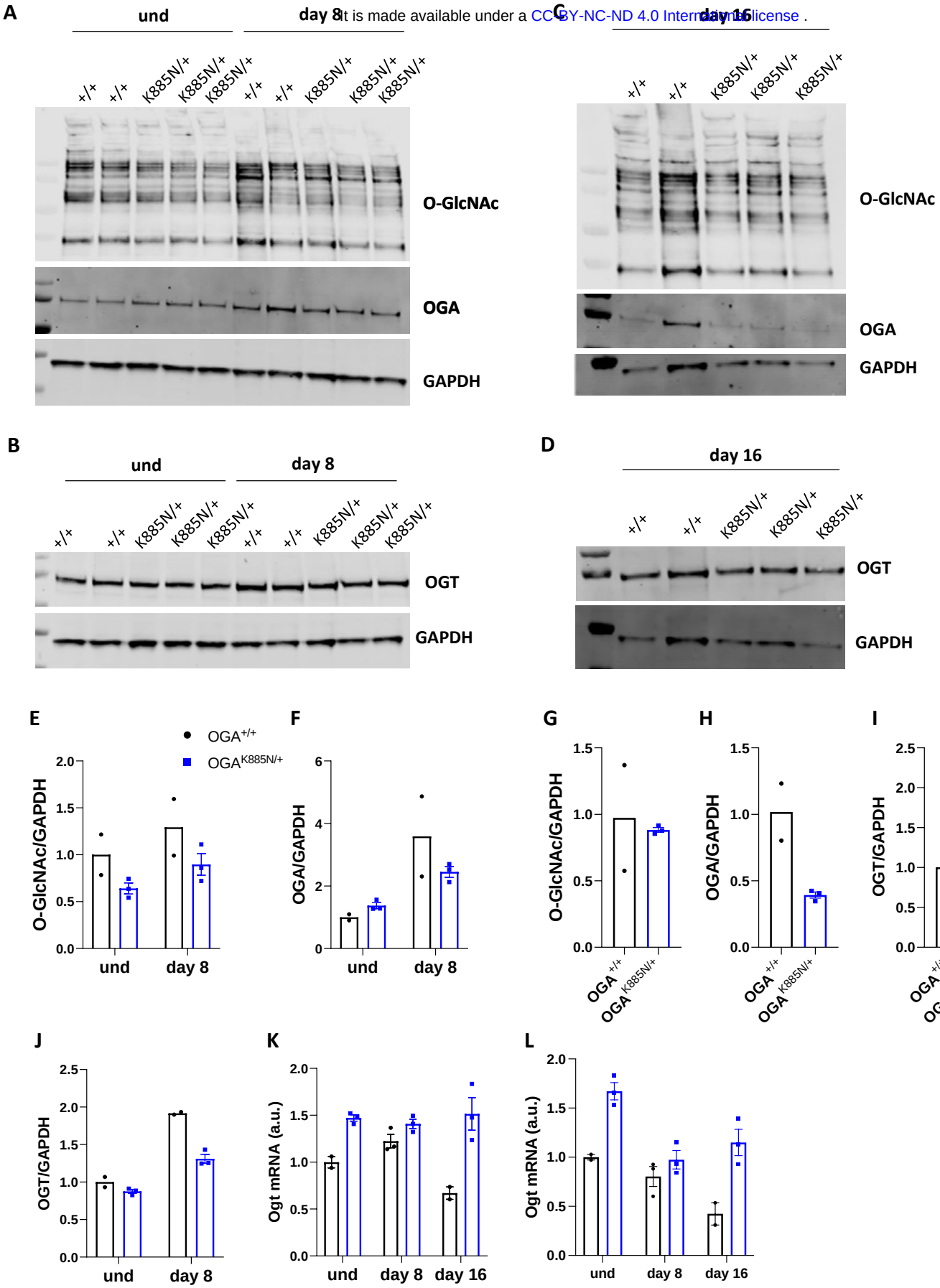

Fig. 4

A

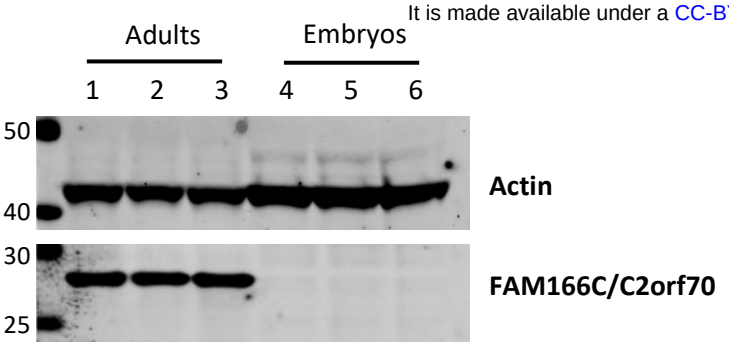

B

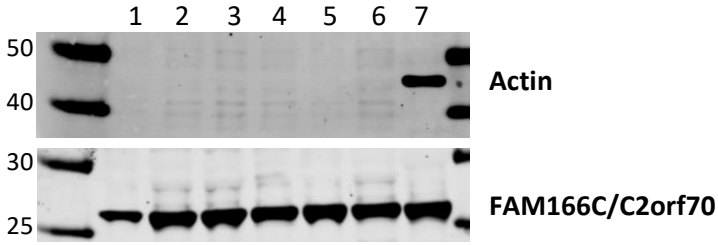

A

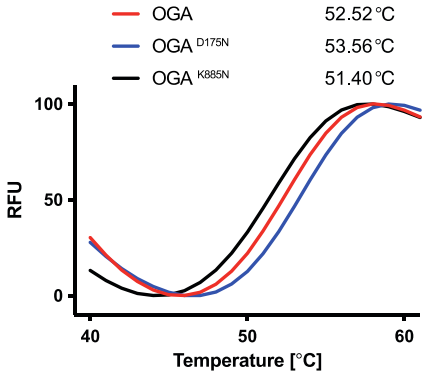

B